BMC Gastroenterology

RESEARCH

Open Access

Dual-phase contrast-enhanced CT-based intratumoral and peritumoral radiomics for preoperative prediction of lymph node metastasis in gastric cancer

Yun-hui Zhou[1,4], Xiao-li Chen[2], Xin Zhang[3], Hong Pu[1†] and Hang Li[1*†]

Abstract

Objective To determine whether intratumoral and peritumoral radiomics derived from dual-phase contrast-enhanced CT imaging could predict lymph node metastasis (LNM) in gastric cancer.

Methods Patients with gastric cancer from January 2017 to January 2022 were retrospectively collected and were randomly divided into training cohort ($n=287$) and test cohort ($n=121$) with a ratio of 7: 3. Clinical features and traditional radiological features were analyzed to construct clinical model. Radiomics features based on intratumoral (ITV) and peritumoral volumetric (PTV) regions of the tumor were extracted and screened to construct radiomics models. Clinical-radiomics combined model was constructed by the most predictive radiomics features and clinical independent predictors. The correlation between LNM predicted by the best model and 2-year disease-free survival (DFS) was evaluated by the Kaplan-Meier analysis.

Results CT-LNM and CT-T stage were independent predictors of LNM. Compared with other radiomics models, ITV + PTV on atrial and venous phase (ITV + PTV-AP + VP) radiomics model presented moderate AUCs of 0.679 and 0.670 in the training cohort and validation cohort, respectively. Among the models, clinical-radiomics combined model achieved the highest AUC of 0.894 and 0.872 in the training and test cohorts, and 0.744 and 0.784 in the T1-2 and T3-4 subgroups, respectively. Clinical-radiomics combined model based LNM could stratify patients into high-risk and low-risk groups, and 2-year DFS of high-risk group was significantly lower than that of low-risk group ($p<0.001$).

Conclusion Clinical-radiomics combined model integrating CT-LNM, CT-T stage, and ITV-PTV-AP + VP radiomics features could predict LNM, and this combined model based LNM was associated with 2-year DFS.

Keywords Radiomics, Lymph node metastasis, Prognosis, Gastric cancer

†Hong Pu and Hang Li contributed equally to this work.

*Correspondence:
Hang Li
lihang111222@126.com
[1]Department of Radiology, Sichuan Provincial People's Hospital, University of Electronic Science and Technology of China, 32# Second Section of First Ring Road, Qingyang District, Chengdu, Sichuan 610072, China
[2]Department of Radiology, Affiliated Cancer Hospital of Medical School, University of Electronic Science and Technology of China, Sichuan Cancer Hospital, Chengdu 610000, China
[3]GE Healthcare (China), 1# Tongji South Road, Daxing District, Beijing 100176, China
[4]Department of Radiology, The Third Affiliated Hospital of Chengdu Medical College•Chengdu pidu District People's Hospital, 666# Second Section of Deyuan North Road, Pidu District, Chengdu, Sichuan 611730, China

Introduction

Gastric cancer is the fifth most common malignant tumor and the third cause of cancer-related death in the world [1, 2]. At present, radical tumor resection is still the main treatment for resectable gastric cancer [3–5]. Despite the improvement of adjuvant therapy, the postoperative survival of gastric cancer remains poor, with a 5-year survival rate of only 20-30% [6, 7]. Local spread of tumor and distant metastasis of cancer cells are the main causes of postoperative recurrence. Therefore, the preoperative assessment of the risks of recurrence might enable personalized treatment in patients with gastric cancer. Lymph node metastasis (LNM) is one of the important factors affecting the cancer staging, the choice of the treatment and prognosis assessment [8, 9]. Accurate preoperative assessment of LNM in gastric cancer patients is very important for optimizing treatment strategies.

The round-like enlarged lymph nodes with a short diameter of ≥ 10 mm on CT image as a criterion for LNM in gastric cancer, but the diagnostic specificity of relying on the size of the lymph nodes alone is poor [10, 11]. Even with advances in CT technology and increasing resolution, the accuracy of conventional CT in the assessment of LNM is only about 62-63% [12, 13]. The possible reason could be that some normal-sized lymph nodes may have micrometastases or some lymph nodes may be enlarged only due to inflammatory response [14, 15]. In recent years, more and more studies have shown the feasibility of radiomics for identifying LNM in gastric cancer [16–19]. However, these studies have mainly focused on the heterogeneity of the tumor itself. Tumor heterogeneity exists not only in tumor cells but also in non-malignant and infiltrating cells surrounding the tumor, often referred to as the peritumoral microenvironment [20]. It has been shown that radiomics features of the peritumoral region correlate with tumor aggressiveness [21]. For gastric cancer, tumor aggressiveness may indicate the presence of LNM and poor prognosis [22]. To our knowledge, few studies exploring the predictive value of CT image-based radiomics features of the peritumoral region for LNM in gastric cancer [23, 24]. In addition, most CT radiomics studies on gastric cancer are mainly based on venous phase (VP) CT image [25]. However, radiomics features based on arterial phase (AP) CT image also have some application value [26–29]. Therefore, we aimed to develop and validate dual-phase contrast enhanced CT-based radiomics from intratumoral and peritumoral tissues for preoperative predicting LNM, and then to determine whether the best predictive model-based LNM was associated with 2-year disease-free survival (DFS) in patients with gastric cancer.

Materials and methods

Patients

The institutional review board approved this retrospective study and waived the requirement for informed consent, aligning the research with the principles of the Declaration of Helsinki. 525 patients with gastric cancer between January 2017 and January 2022 were retrospectively enrolled in this study. The inclusion criteria consisted of (a) pathologically confirmed primary gastric cancer; (b) performing radical tumor resection; (c) undergoing contrast enhanced CT examination before surgery; and (d) without other synchronous malignant tumors. 117 patients were excluded for the following reasons: (a) receive neoadjuvant treatment prior to surgery ($n = 66$); (b) poor image quality due to severe artifacts and distortion ($n = 14$) (c) the maximal diameter of tumor was less than 6 mm, insufficient to place a valid volume of interest (VOI) ($n = 37$). The remaining 408 patients (275 men, 133 women; mean age, 62.0 ± 11.77 years) were finally enrolled in this study (Fig. 1). All cases were divided into training group and test group by stratified random sampling at a ratio of 7:3.

Imaging protocol

The patients were told to make gastrointestinal preparations before the CT examination, to abstain from solid food for 6–8 h, and to inject 654-2 intramuscularly 30 min before the examination to inhibit intestinal peristalsis, and to drink 800–1600 mL of water 10 min before the examination to adequately dilate the gastric lumen. The Dual-energy CT (SOMATOM Force; Siemens Healthineers, Forchheim, Germany) scanner was used for the examination. The acquisition parameters for contrast enhanced CT were as follows: 120/130 kV tube voltage, automated tube current, scanning layer thickness and layer spacing of 5–8 mm, reconstruction section thickness of 3 mm, matrix 512 × 512. Iohexol (Omnipaque, GE Healthcare, 350 mg iodine/ml) was injected into the cubital vein at a dose of 1.2–1.5 mL/kg and at a rate of 2-3mL/s. Intelligent triggering technology determined the time of AP scanning. The AP scan was triggered by an automatic threshold (120 HU), and VP image acquisition was performed after a 30s delay.

Clinical and pathological data

Clinical data included age, gender, CA199 and CEA. All patients underwent radical tumor resection, and the surgical resection specimens were treated with 10% formalin for conventional fixation and stained with hematoxylin-eosin. Pathologists evaluated and recorded the biopsy/surgical specimens according to the AJCC 8th edition gastric cancer staging criteria [30]. The criteria for determining LNM as follows: the presence of cancer cells in

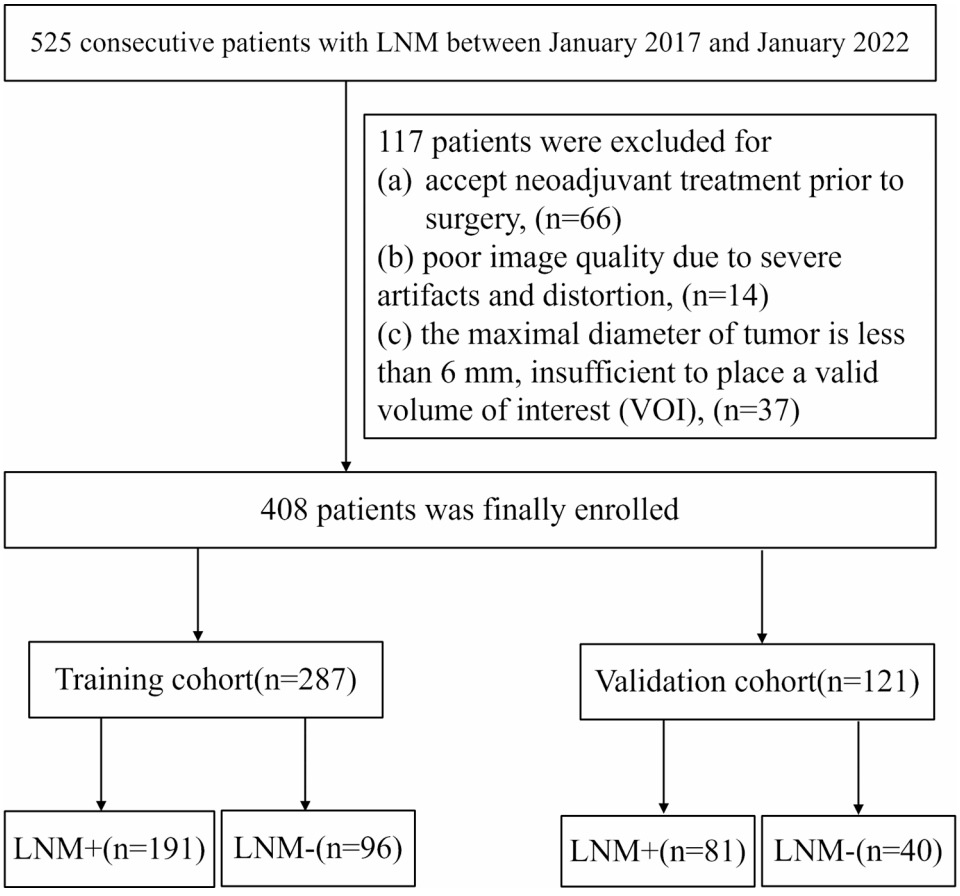

Fig. 1 Flowchart of patient selection

lymph nodes as indicated by the routine pathohistological examination results.

Traditional CT radiological feature analysis

The subjective CT features for each patient were independently evaluated and recorded by a radiologist (the first author, with 3 years of experience in gastric cancer, respectively) and confirmed by another senior radiologist (with more than 10 years of experience in gastric cancer). The two radiologists were blinded to the histopathology and the clinical history. If the results were inconsistent, a third senior radiologist (with more than 20 years of experience in gastric cancer) would be involved to resolve the issue. Subjective CT features were recorded on venous-phase CT imaging as follows:

(1) thickness of the tumor, measured at the maximal thickness of the tumor on transverse CT imaging; (2) maximum diameter of tumor, measured at the tumor's largest cross-sectional area on transverse CT imaging; (3) T-staging, defined as the depth of primary tumor infiltrating into the gastric wall; (4) The tumor sites included the upper 1/3, middle 1/3, lower 1/3, and ≥2/3 regions of the stomach. CT lymph node status assessment criteria: regional lymph node diameter > 10 mm, or with heterogeneous enhancement, or ≥3 clusters of lymph nodes considered LNM [31].

Image processing and tumor segmentation

The acquired thin-layer CT images were transferred to a Siemens post-processing workstation (Syngo.via, Version VB10B; Siemens) for image reconstruction, with the reconstructed layer thickness and the reconstructed layer spacing of 3 mm. The reconstructed images were imported into the medical image visualization software ITK-SNAP (www.itksnap.org) in DICOM format. A radiologist (the first author) manually defined the entire tumor region of interest (ROI) on the VP CT images. This ROI was then applied to the AP CT images, and slightly adjusted according to the specific conditions when necessary to obtain the AP intratumoral ROI. For segmentation of the peri-tumor region, the tumor border was expanded outward by 2 mm and contracted inward by 1 mm to obtain a 3-mm region around the tumor, and the peritumoral ROI in the VP and AP were obtained by layer-by-layer outlining [24]. The air visible to the naked eye and the surrounding large blood vessels and parenchymal organs were avoided as much as possible. The outlined images were finally fused into 3D

regions automatically. The tumor segmentation process was shown in Fig. 2.

Fifty patients were randomly selected from 408 patients to assess interobserver and intraobserver agreement of feature extraction by intraclass correlation coefficient (ICC) analysis. The same radiologist delineated the volumetric ROI and repeated this process after one month to calculate the intraobserver ICC. The two radiologists delineated the volumetric ROI to calculate the interobserver ICC. The radiomics features with ICC coefficients greater than 0.8 indicated good stability and reliability [32].

Radiomics feature extraction, selection and model construction

Radiomics features were extracted using the Pyradiomics software package. Voxel size was resampled by $1 \times 1 \times 1$ mm, and Z-score normalization for CT images were performed using PyRadiomics. A total of 1037 radiomics features were calculated for original images and filtered images from each sequence. The R software (version 3.5.1, https://www.r-project.org/) was used to filter the radiomics features from the radiomics pool and build the model. The Max-Relevance and Min-Redundancy (mRMR) and least absolute shrinkage and selection operator (LASSO) regression were used to select the optimized subset of features. Based on the radiomics features selected from different regions, the radiomics models were established as follows: intratumoral radiomics model in arterial phase (ITV-AP model), peritumoral radiomics model in arterial phase (PTV-AP model), intratumoral radiomics model in venous phase (ITV-VP model), peritumoral radiomics model in venous phase (PTV-VP model), intratumoral and peritumoral radiomics model in arterial phase (ITV + PTV-AP model), intratumoral and peritumoral radiomics model in venous stage (ITV + PTV-VP model), intratumoral radiomics model in arteriovenous stage (ITV-AP + VP model), peritumoral radiomics model in arteriovenous stage (PTV-AP + VP model), intratumoral and peritumoral radiomics model in arteriovenous stage (ITV + PTV-AP + VP model). Selected features were weighted by their respective coefficients to construct a radiomics signature score (Radscore) for predicting LNM, and the most predictive Radscore was selected for subsequent analyses by comparing the AUC values of the models for predicting LNM in the training cohort.

To further determine whether the radiomics model is overfitting, principal component analysis (PCA) is performed on the features that included in the radiomics model. And then those representative features of each component were used to construct the radiomics model.

The clinical model, nomogram construction and evaluation

The most predictive radiomics signatures, clinical factors, and subjective CT features were used to establish the combined clinical-radiomics model by univariate and multivariate logistic regression analyses. A nomogram was generated for providing a clinical applicable tool for predicting LNM. The receiver operating characteristic (ROC) curves were used to assess the discriminative performance of the models. Calibration curves were used to assess the goodness of fit of the models. The Delong test was used to compare the differences in AUC values between models. The clinical utility of the models was assessed by quantifying the net benefit at different threshold probabilities by decision curve analysis (DCA). Workchart of key steps to build a combined clinical-radiomics model (Fig. 3).

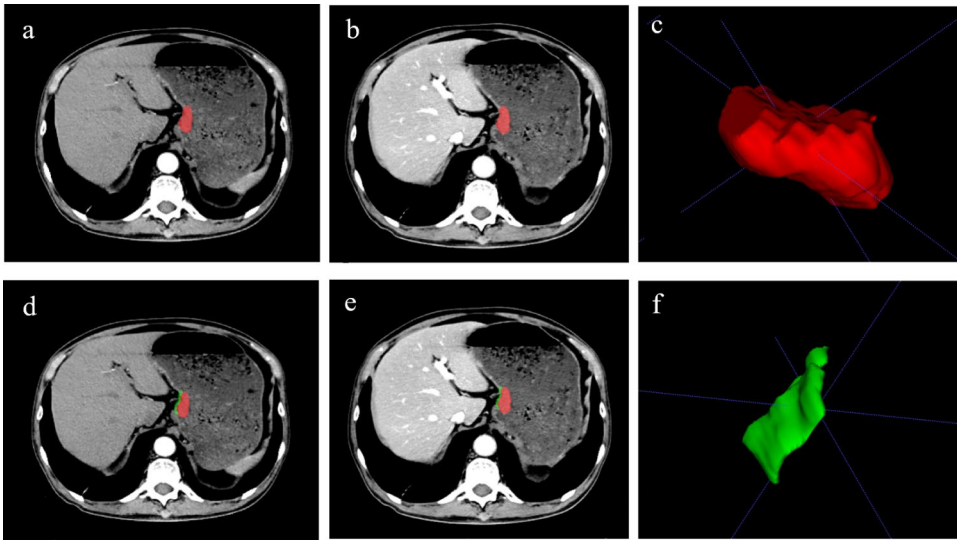

Fig. 2 Lesion segmentation in dual-phase contrast-enhanced CT images of a typical gastric cancer

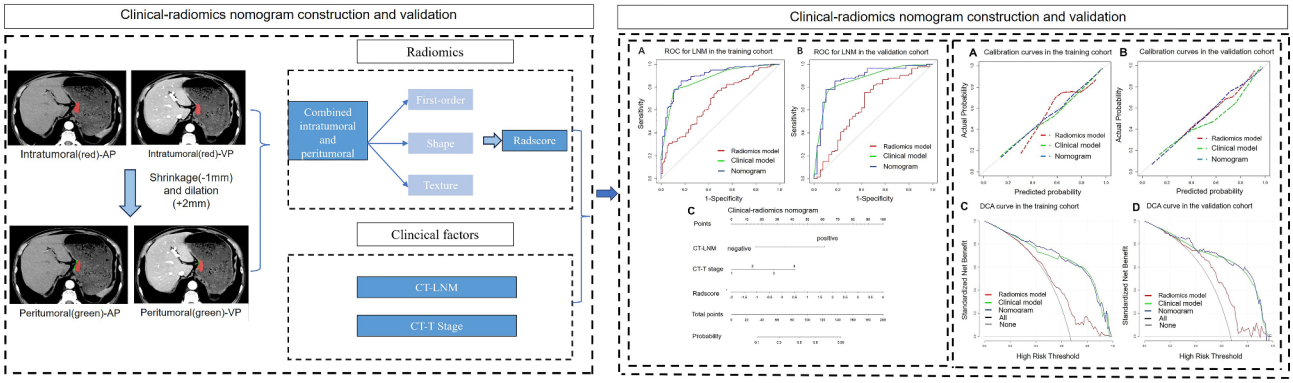

Fig. 3 Workchart of key steps to build a clinical-radiomics model

Prognosis evaluation

Patients were followed up every 3–6 months after surgery using endoscopic examination plus CT, MRI, and laboratory examination. 2-year DFS was used as the endpoint of this study, which referred to the time interval from gastric cancer surgery to tumor recurrence/metastasis or death of patients due to gastric cancer-related causes. Independent risk factors for 2-year DFS after radical tumor resection in gastric cancer patients were determined by univariate and multivariate Cox regression analysis. Kaplan-Meier analysis and log-rank test were used to plot survival curves and compare differences between groups, and to stratify gastric cancer patients.

Statistical analysis

SPSS software (version: 23.0) and R software were used for statistical analysis. Comparisons between groups were performed using the independent two-sample t test or Mann-Whitney U test. Qualitative data was expressed as frequencies (percentages) and comparisons between groups were made using the chi-square test. The ROC curve was drawn and the diagnostic performance was evaluated by the AUC. The comparison of AUCs between the models were determined by Delong's test. Univariate and multivariate Cox regression analyses were performed to build a prognostic model for assessing 2-year DFS. Kaplan-Meier analysis and log-rank test were used to plot survival curves. A two-sided $p < 0.05$ was set as statistically significant difference.

Results

Baseline characteristics

A total of 408 patients (mean age, 62.0 ± 11.77 years; range 18–88 years) were included in this study, of which 277 were LNM positive and 131 were LNM negative. All cases were divided into training group (191 LNM-positive and 96 LNM-negative) and test group (81 LNM-positive and 40 LNM-negative) by stratified random sampling at a ratio of 7:3.

Clinical baseline data between LNM-positive and LNM-negative patients in the training and test groups are shown in Table 1. There was significant difference in tumor differentiation between pathological LNM-positive and LNM-negative patients in the training group ($p < 0.001$) whereas no significant difference was found in the test group ($p = 0.106$). There were significant differences in tumor maximum diameter, CT-T stage, and CT-LNM between pathological LNM-positive and LNM-negative patients (all $p < 0.001$).

Clinical model construction

As shown by univariate and multivariate logistic regression analysis, CT-LNM ($p < 0.001$) and CT-T stage ($p < 0.001$) were independent risk factors for predicting LNM in gastric cancer. A clinical model was established based on these independent risk factors, and the model scoring formula was shown as follows: Clinical model score=-1.822 + 2.955×CT-LNM + 0.709×CT-T stage.

Evaluation of model performance

The specific radiomics features and the corresponding calculation formulas are shown in Table S1. ITV + PTV-AP + VP radiomics model achieved better AUC than that of the other radiomics model. A combined clinical-radiomics model is constructed by adding ITV + PTV-AP + VP radscore to the clinical factor (Table 2). The diagnostic performance of models in the training and test groups are shown in Table 3. The nomogram is constructed for visualizing the combined model (Fig. 4). The ROC curves for the clinical model, radiomics model and clinical-radiomics combined model are shown in Fig. 4. The combined model achieved slightly higher AUC than that of clinical model (AUC, 0.894 vs. 0.874, in the training cohort, $p = 0.02$; 0.872 vs. 0.867 in the test cohort, $p = 0.7$) and ITV + PTV-AP + VP radiomics model (AUC, 0.894 vs. 0. 679 in the training cohort, $p < 0.001$; 0.872 vs. 0.670 in the test cohort, $p < 0.001$). The clinical model achieved higher AUC than that of ITV + PTV-AP + VP radiomics model (AUC, 0.874 vs.

Table 1 Comparison of clinical features between training group and test group

Characteristics	Training group($n=287$)			Test group($n=121$)		
	LNM-($n=96$)	LNM+($n=191$)	*p*	LNM-($n=40$)	LNM+($n=81$)	*p*
Age(year)			0.588			0.400
≤60	40(41.7%)	84(44.0%)		18(45.0%)	41(50.6%)	
>60	56(58.3%)	107(56.0%)		22(55.0%)	40v49.4%)	
Gender			1.000			0.699
Male	65(67.7%)	130(68.1%)		25(62.5%)	55(67.9%)	
Female	31(32.3%)	61(31.9%)		15(37.5%)	26(32.1%)	
Differentiation			< 0.001			0.106
Poor/undifferentiated	56(58.3%)	152(79.6%)		29(72.5%)	70(86.4%)	
Well/moderate	40(41.7%)	39(20.4%)		11(27.5%)	11(13.6%)	
CA199			0.163			0.272
Normal (≤5.0ug/ml)	84(87.5%)	153(80.1%)		36(90.0%)	65(80.2%)	
Elevated (>5.0ug/ml)	12(12.5%)	38(19.9%)		4(10.0%)	16(19.8%)	
CEA			0.136			0.587
Normal (≤37.0U/ml)	84(87.5%)	152(79.6%)		34(85.0%)	64(79.0%)	
Elevated (>37.0U/ml)	12(12.5%)	39(20.4%)		6(15.0%)	17(21.0%)	
Tumor location			0.058			0.108
upper 1/3	4(0.1%)	28(14.7%)		9(22.5%)	7(8.6%)	
middle 1/3	23(24.0%)	36(18.8%)		11(27.5%)	21(25.9%)	
lower 1/3	29(30.2%)	56(29.3%)		16(40.0%)	43(53.1%)	
≥2/3	40(41.7%)	71(37.2%)		4(10.0%)	10(12.4%)	
Tumor maximum diameter			< 0.001			< 0.001
≤40 mm	84(87.5%)	41(21.5%)		26(65%)	21(25.9%)	
>40 mm	12(12.5%)	150(78.5%)		14(35%)	60(74.1%)	
Tumor thickness (mm)	15.6 ± 8.69	16.8 ± 7.43	0.258	14.5 ± 7.30	18.2 ± 16.1	0.085
CT-T stage			< 0.001			< 0.001
T1	29(30.2%)	7(3.6%)		10(25.0%)	1(1.2%)	
T2	16(16.7%)	16(8.4%)		7(17.5%)	7(8.7%)	
T3	43(44.8%)	126(66.0%)		19(47.5%)	49(60.5%)	
T4	8(8.33%)	42(22.0%)		4(10.0%)	24(29.6%)	
CT-LNM			< 0.001			< 0.001
negative	84(87.5%)	41(21.5%)		35(87.5%)	18(22.2%)	
positive	12(12.5%)	150(78.5%)		5(12.5%)	63(77.8%)	

Note: CA199, carbohydrate antigen 199; CEA, carcinoembryonic antigen; CT, Computed Tomography; LNM, lymph node metastasis

Table 2 Univariate and multivariate logistic regression analyses of characteristic variables for predicting lymph node metastasis in training group

Characteristics	Univariate analysis			Multivariate analysis		
	OR	95%CI	*p*	OR	95%CI	*p*
Age	0.85	0.51–1.41	0.298			
Gender	0.98	0.58–1.66	0.579			
CEA	1.80	0.89–3.62	0.604			
CA199	1.74	0.86–3.51	0.093			
Differentiation	0.40	0.25–0.63	<0.001			
Tumor location	1.28	0.98–1.67	0.652			
Tumor maximum diameter	2.36	1.43–3.90	<0.001			
Tumor thickness	1.02	0.99–1.06	0.235			
CT-T stage	2.93	2.10–4.09	<0.001	1.91	1.28–2.86	< 0.001
CT-LNM	25.61	12.76–51.39	<0.001	17.58	8.51–36.35	< 0.001
ITV + PTV-AP + VP Radscore	2.72	1.84–4.02	<0.001	2.17	1.29–3.67	0.002

Note: CT, Computed Tomography; LNM, lymph node metastasis; ITV, intratumoral volume; PTV, peritumoral volume; AP, arterial phase; VP, venous phase

Table 3 Diagnostic efficacy of models

Model	AUC	95%CI	ACC	SPE	SEN
Training group					
ITV-AP radiomics model	0.670	0.603–0.736	0.683	0.573	0.738
ITV-VP radiomics model	0.655	0.589–0.722	0.648	0.573	0.686
PTV-AP radiomics model	0.613	0.544–0.682	0.617	0.635	0.607
PTV-VP radiomics model	0.657	0.591–0.723	0.669	0.669	0.669
ITV + PTV-AP radiomics model	0.679	0.616–0.743	0.659	0.573	0.702
ITV + PTV-VP radiomics model	0.657	0.591–0.723	0.669	0.552	0.552
ITV-AP + VP radiomics model	0.676	0.612–0.740	0.645	0.604	0.665
PTV-AP + VP radiomics model	0.655	0.589–0.722	0.648	0.573	0.686
ITV + PTV-AP + VP radiomics model	0.679	0.615–0.744	0.686	0.521	0.770
Clinical model	0.874	0.834–0.914	0.812	0.896	0.770
Nomogram	0.894	0.855–0.933	0.847	0.833	0.853
Test group					
ITV-AP radiomics model	0.600	0.489–0.711	0.628	0.400	0.741
ITV-VP radiomics model	0.665	0.552–0.778	0.669	0.575	0.716
PTV-AP radiomics model	0.661	0.552–0.771	0.661	0.600	0.691
PTV-VP radiomics model	0.660	0.548–0.773	0.694	0.550	0.765
ITV + PTV-AP radiomics model	0.633	0.521–0.746	0.702	0.550	0.778
ITV + PTV-VP radiomics model	0.660	0.548–0.773	0.694	0.550	0.765
ITV-AP + VP radiomics model	0.655	0.543–0.768	0.661	0.550	0.716
PTV-AP + VP radiomics model	0.665	0.552–0.778	0.669	0.575	0.716
ITV + PTV-AP + VP radiomics model	0.670	0.538–0.760	0.694	0.500	0.790
Clinical model	0.867	0.799–0.934	0.810	0.875	0.778
Nomogram	0.872	0.799–0.945	0.835	0.775	0.864

Note: AUC, the area under the receiver operating characteristic curve; CI, confidence intervals; ITV, intratumoral volume; PTV, peritumoral volume; AP, arterial phase; VP, venous phase; ACC, Accuracy; SPE, Specificity; SEN, Sensitivity

0.679, in the training cohort, $p < 0.001$; 0.867 vs. 0.670 in the test cohort, $p < 0.001$). The calibration curves and decision curves of the three models in the training and test groups are shown in Fig. 5, respectively. The calibration curves showed that the combined clinical-radiomics model had the best fit in the training and testing groups. DCA showed that the overall net benefit achieved by the clinical- radiomics combined model was similar with that of the clinical model, and was higher than that of the ITV + PTV-AP + VP radiomics model in a large range of threshold probabilities (training group, 0.18–0.98; test group, 0.22–0.97).

PCA

As for PCA results, 5 of 8 principal components in ITV + PTV-AP + VP radiomics model contributed more than 10%. Therefore, those representative features of each component were used to construct the radiomics model. The AUC, accuracy, specificity and sensitivity for radiomics model was 0.674 (0.608–0.741), 0.676, 0.594, and 0.717, respectively in the training group and 0.666 (0.525–0.747), 0.656, 0.550, and 0.679, respectively in the test group.

Subgroup analysis

All cases were divided into T1-T2 and T3-T4 subgroups according to the pathologic T stage. In the T1-T2 group, there were 31 LNM-positive cases (33.33%) and 62 LNM-negative cases (66.67%). In the T3-T4 group, there were 241 LNM-positive cases (76.51%) and 74 LNM-negative cases (23.49%). The LNM-positive rate increased significantly with the increasement of T stage. The diagnostic performance of the clinical-radiomics combined model for LNM in different subgroups is shown in Table 4. In the T1-2 and T3-4 subgroups, the AUC of the combined clinical-radiomics model was 0.744 and 0.784 for predicting LNM, respectively.

Prognostic analysis

The median follow-up time for all patients was 24 months (range, 1–24 months). Of the 408 patients, 146 patients (35.8%) experienced recurrence or died from gastric cancer-related causes at a median follow-up time of 7 months (range, 1–24 months). Univariate and multivariate Cox regression analysis showed that age, CT-LNM, and the combined clinical-radiomics model-based LNM were independent risk factors (Table 5). Kaplan-Meier analysis showed both pathologic LNM and combined clinical-radiomics model-based LNM were associated with postoperative 2-year DFS and could stratify the patients into low-risk and high-risk group (all $p < 0.001$) (Fig. 6). Patients with pathologic LNM-positive had lower 2-years DFS rates than that of LNM-negative (55.9% vs. 86.8%, $p < 0.001$). Meanwhile, patients with LNM-positive predicted by the combined clinical-radiomics model also had lower 2-years DFS rates than that of LNM-negative (51.6% vs. 83.7%, $p < 0.001$).

Discussion

Evaluation of lymph node status in gastric cancer depending solely on CT morphological features remains challenging at present. The accuracy of conventional CT for the assessment of LNM in gastric cancer was only 62-63% [12, 13]. Radiomics features based on tumor regions on CT images could predict LNM in early gastric cancer with AUC of 0.850 [33]. In this study, we found intratumoral radiomics model could predict LNM

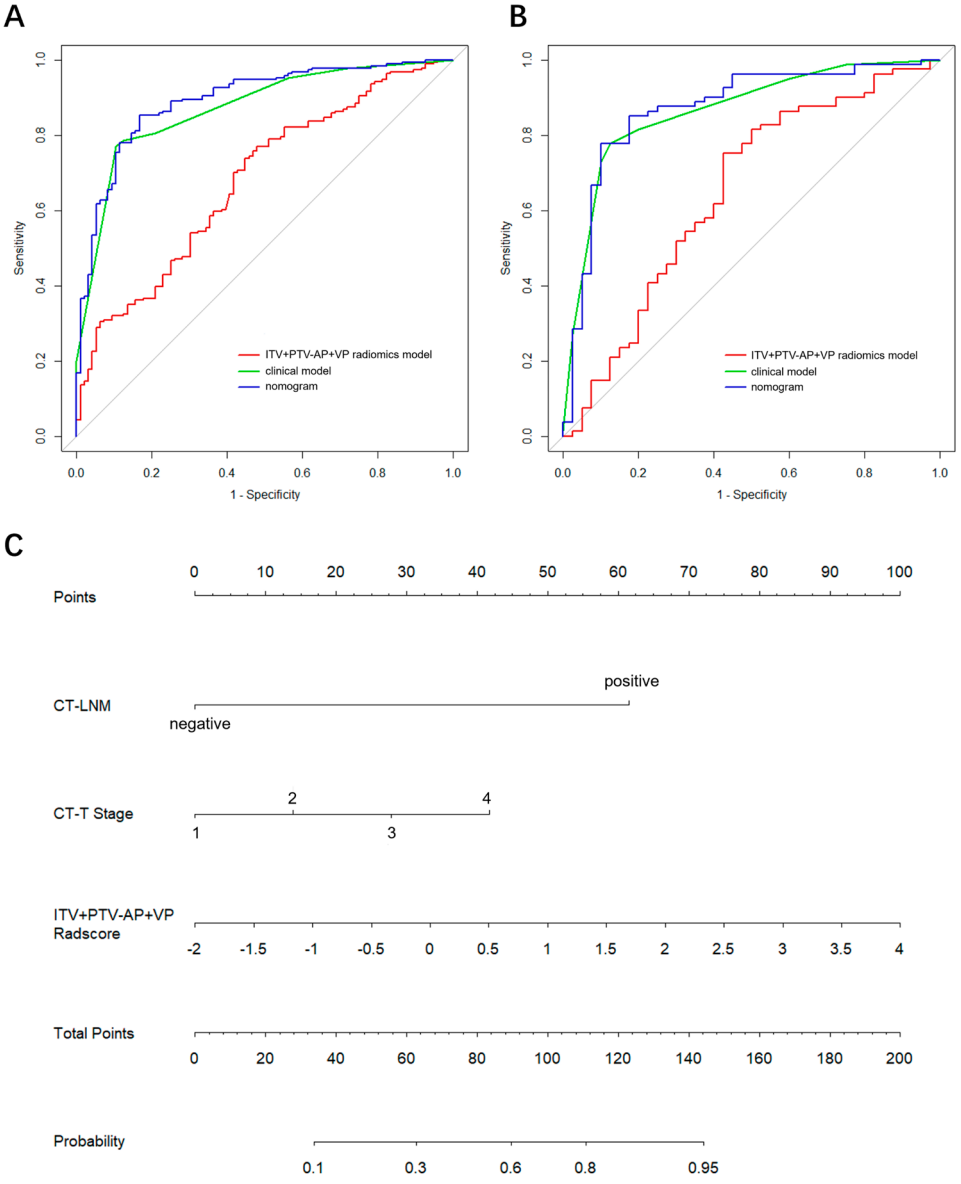

Fig. 4 Receiver operating characteristic curves of radiomics model, clinical model and clinical-radiomics nomogram for predicting lymph node metastasis (LNM) of gastric cancer in the training cohort (**A**) and validation cohort (**B**). The nomogram is constructed for visualizing the combined model (**C**)

in gastric cancer with AUCs of 0.600 for ITV-AP, 0.665 for ITV-VP, and 0.655 for ITV-AP + VP, respectively. The predictive performance of intratumoral radiomics model was lower than that of previous study. The possible reason could be that early and advanced gastric cancer were both included in this study and tumors with different T-stages may have a potential impact on the LNM. Yang et al. reported that combining intratumoral and peritumoral radiomics model showed better AUC than that of intratumoral radiomics model (AUC, 0.724 vs. 0.710) [14]. Our study also showed radiomics model based on intratumoral and peritumoral region showed better AUC in both arterial (0.679 vs. 0.670) and venous (0.657 vs. 0.655) phases compared with intratumoral radiomics model alone. However, the AUC in this study was lower than Yang et al. findings, which may be attributed to the fact that the selection of peritumoral region was different (3 mm vs. 5 mm). In this study, we chose 3 mm as peritumoral region because previous studies demonstrated that 3 mm peritumoral area provides significant information for assessing the immune microenvironment in gastric cancer [34, 35]. In future studies, it would be beneficial to investigate the impact of varying peritumoral region ranges (e.g., 3 mm, 5 mm, or even larger) on the predictive performance for LNM.

The ITV + PTV-AP + VP model incorporated eight radiomics features. Two of the main features, Elongation and Sphericity, were from the intratumoral region.

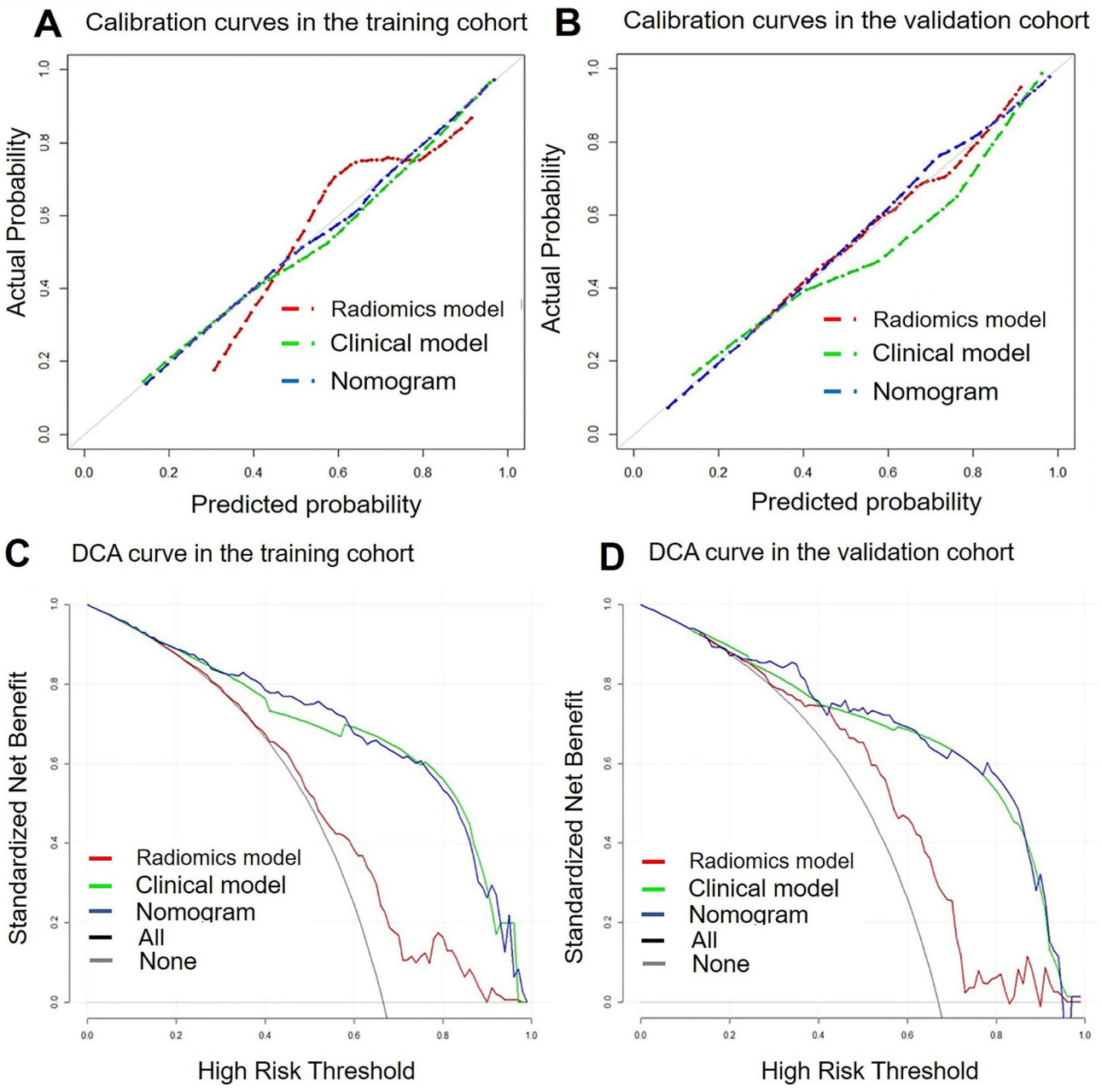

Fig. 5 The calibration curve of the three models in the training cohort (A) and validation cohort (B) for predicting lymph node metastasis (LNM). The decision curve analysis curves of the three models in the training cohort (C) and validation cohort (D) for predicting LNM

Table 4 Subgroup analysis of the clinical-radiomics combined model for predicting lymph node metastasis

Subgroup	AUC	95%CI	SPE	SEN
T1-2	0.744	0.668–0.891	69.2%	71.5%
T3-4	0.784	0.452-1.000	93.7%	80.0%

AUC, the area under the receiver operating characteristic curve; CI, confidence intervals; SPE, Specificity; SEN, Sensitivity

Elongation is one of the shape features showing the relationship between the two largest principal components in the shape of the ROI [36]. Sphericity indicates the roundness of the tumor region with respect to the shape of the sphere. The negative coefficients of Elongation and Sphericity indicate the irregular of the tumor. When the tumor is more irregular, its invasiveness tends to be higher and metastatic tumor cells have a stronger ability to reach the proximal and distal lymph node through lymphatic drainage [37]. Moreover, we also found that the radiomics features of the peritumoral region showed

Table 5 Univariate and multivariate Cox regression analyses based on all cases

VarName	Univariate analysis			Multivariate analysis		
	p	HR	95%CI	*p*	HR	95%CI
Age(> 60 years)	0.378	0.783	0.455–1.349			
Gender(female)	0.038	2.113	1.042–4.287	0.031	2.047	1.066–3.932
CEA(> 5.0*ng/ml*)	0.272	0.684	0.348–1.347			
CA199(> 37.0*U/ml*)	0.063	0.550	0.293–1.033			
Differentiation (Poor/undifferentiated)	0.601	1.185	0.628–2.236			
CT-T stage(T3-4)	0.062	0.288	0.078–1.062			
Tumor maximum Diameter(> 40 mm)	0.756	0.899	0.458–1.762			
Tumor thickness (> 15 mm)	0.509	1.416	0.504–3.972			
Tumor location						
middle 1/3	1.000	1.000	0.200-5.002			
lower 1/3	0.917	0.927	0.224–3.833			
≥ 2/3	0.012	2.912	1.264–6.704	0.113	1.022	0.568–2.442
CT-LNM	0.005	0.376	0.189–0.749	< 0.001	0.236	0.123–0.452
LNM predicted by combined clinical- radiomics model	0.006	0.404	0.211–0.775	0.042	0.547	0.305–0.979

HR, hazard ratio; CI, confidence interval; CEA, carcinoembryonic antigen; CA199, carbohydrate antigen 199; CT, Computed Tomography; LNM, lymph node metastasis. Gender (male), age (≤ 60), CA199 (≤ 37.0U/ml), CEA (≤ 5.0ng/ml), Differentiation (Well/moderate), CT-T stage (T1-2), Tumor maximum diameter (≤ 40 mm), Tumor thickness (≤ 15 mm), Tumor location(upper 1/3) and clinical-radiomics combined model-based LNM (negative) were as a reference in univariate and multivariate COX analysis

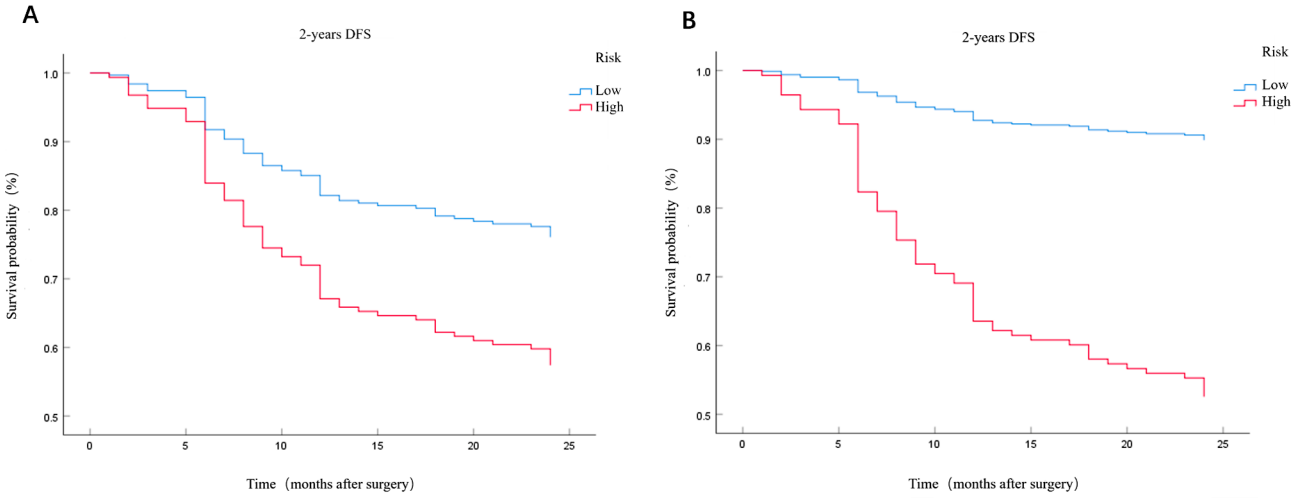

Fig. 6 Kaplan-Meier analysis of the nomogram-based lymph node metastasis (**A**) and pathological lymph node metastasis (**B**) for predicting 2-year disease-free survival (DFS) in patients with gastric cancer in the whole groups

some significance, which were correlated with the inhomogeneity of the image texture and might indirectly reflect the heterogeneity of the tumor. In this study, radiomics model based on PCA achieved similar diagnostic performance with ITV + PTV-AP + VP radiomics model (AUC, 0.666 vs. 0.670). This result may indicate there is not significant overfitting for ITV + PTV-AP + VP radiomics model.

Some studies reported that lymph node status and CT-T stage were independent risk factors for assessing LNM in gastric cancer [13, 38]. With the increasing depth of tumor infiltration, lymphovascular-rich areas tend to be more easily invaded, which in turn promotes LNM [39]. In this study, we also found CT-T stage and CT-LNM are independent risk factors for predicting LNM. Previous studies have shown that in the absence of reliable factor to predict LNM in gastric cancer, radiomics features combined with clinical risk factors are viable alternatives [40]. In this study, we also combined the clinical risk factors with the radiomics signatures to construct a clinical-radiomics nomogram. Compared with clinical model and radiomics model, we found that combined clinical-radiomics model constructed by combining CT-T stage and CT-LNM with the most predictive radscore showed the best diagnostic performance (AUC = 0.872). Although there was no statistically

significant difference for AUC between the combined model and the clinical model, the sensitivity and accuracy of the combined model further improved (sensitivity, 0.853 vs. 0.770; accuracy, 0.847 vs. 0.812). The sensitivity of CT for detecting LNM was lower, especially in T1-T2 stage because the evaluation of lymph node status by CT images mainly relies on morphological features and most of the lymph node size in T1-T2 stage was normal [25, 41]. On the contrary, radiomics signature was not influenced by T staging and still maintained high sensitivity for predicting LNM [42]. Therefore, when combining clinical factors and radiomics features further improved the sensitivity and accuracy because they are not completely identical and could complement each other. We further evaluated the diagnostic performance of the clinical-radiomics combined model for LNM in gastric cancer patients with different T-stages. The results showed that the clinical-radiomics combined model still had a good ability to preoperative identify LNM in the T1-2 stage subgroup and the T3-4 stage subgroup, with the AUC of 0.744 and 0.784, respectively.

Currently, the TNM staging system is still the most reliable method for assessing the prognosis, but this information is mainly obtained through postoperative pathologic specimens. We found that LNM predicted based on a combined clinical-radiomics model could stratify patients into high-risk and low-risk group. High-risk patients had a lower 2-year DFS than that of low-risk patients (51.6% vs. 83.7%). The standard treatment for gastric cancer is radical tumor resection with or without regional lymph node dissection and postoperative chemotherapy if necessary. Although the effectiveness of neoadjuvant therapy is still controversial in gastric cancer [38], some studies have shown that high-risk patients with gastric cancer are more suitable for neoadjuvant therapy [43]. The results of this study showed that LNM predicted based on a combined clinical-radiomics model could make preoperative risk stratification, which may help to identify patients with early recurrence or metastasis.

There were some limitations in this study. First, the results were evaluated at a single center. Extending the results to multiple centers is a need for future study. Second, only arterial-phase and venous-phase CT images were included in this study for radiomics analysis, and delayed-phase CT was not included. Third, it is possible that images acquired using different machines and parameters may affect radiomics characteristics. However, in clinical practice, different centers perform different protocols, which can relatively improve the repeatability of multicenter studies. Fourth, a 3-mm area around the tumor was selected as peritumoral region, although various peritumoral region should be compared and the optimal peritumoral region should be determined in the future. At last, delayed phase CT imaging was not included in this study. Future studies incorporating delayed phase CT imaging should be performed to predict LNM in gastric cancer.

Conclusion

This study demonstrated that a combined clinical-radiomics model integrating intratumoral and peritumoral radiomics features of preoperative dual-phase contrast-enhanced CT and conventional radiological features has the potential to predict LNM. The LNM predicted by the corresponding combined model can be used to assess the 2-year postoperative DFS and stratify patients. In the future, integrating radiomics predictive models for predicting LNM in gastric cancer into medical imaging management systems or hospital clinical decision support systems could help clinicians intuitively view the predicted results for LNM and make the best individualized treatment plan for patients with gastric cancer.

Abbreviations

ACC	Accuracy
AIC	Akaike Information Criterion
AJCC	American Joint Committee on Cancer
AP	Arterial Phase
AUC	Area Under the Curve
CA199	Carbohydrate Antigen 199
CEA	Carcinoembryonic Antigen
CI	Confidence Interval
CT	Computed Tomography
DCA	Decision Curve Analysis
DFS	Disease-free Survival
HR	Relative Risk
ICC	Inter-observer Correlation Coefficient
IDN	Inverse Difference Normalized
ITV	Intratumoral Volume
K-S	Kolmogorov-Smirnov
LASSO	Least Absolute Shrinkage and Selection Operator
LNM	Lymph Node Metastasis
mRMR	Max-Relevance and Min-Redundancy
NCCN	National Comprehensive Cancer Network
PTV	Peritumoral Volume
Radscore	Radiomics score
ROC	Receiver Operating Characteristic
ROI	Region of Interest
SEN	Sensitivity
SPE	Specificity
VP	Venous Phase
PCA	Principal component analysis

Supplementary Information

The online version contains supplementary material available at https://doi.org/10.1186/s12876-025-03728-y.

Supplementary Material 1

Acknowledgements

None.

Author contributions
Yunhui Zhou and Xiaoli Chen contributed to the conception and design of the study, the analysis and interpretation of the data, and the work draft. Xin Zhang and Hong Pu participated in the data collection. Hang Li offered guidance in study design and revised the manuscript critically for important intellectual content. All authors have read and approved the final version of the manuscript.

Funding
None.

Data availability
No datasets were generated or analysed during the current study.

Declarations

Ethics approval and consent to participate
The institutional review board of Sichuan Provincial People's Hospital (No. 2021086) approved this retrospective study and waived the requirement for informed consent, aligning the research with the principles of the Declaration of Helsinki.

Consent for publication
Not applicable.

Competing interests
The authors declare no competing interests.

Received: 4 January 2025 / Accepted: 24 February 2025
Published online: 28 February 2025

References

1. Chandarana CV, Mithani NT, Singh DV, Kikani UB. Vibrational spectrophotometry: A comprehensive review on the diagnosis of gastric and liver Cancer. Curr Pharm Anal. 2024;20:453–65.
2. Fatima S, Song Y, Zhang Z, Fu Y, Zhao R, Malik K, Zhao L. Exploring the Pharmacological mechanisms of P-hydroxylcinnamaldehyde for treating gastric cancer: A Pharmacological perspective with experimental confirmation. Curr Mol Pharmacol. 2024;17:23.
3. Wang Y, Chen S, Yu P, Bao Z, Hu C, Xia Y, Zhang R, Yuan L, Ruan H, Sun J. SR-BI expression regulates the gastric cancer tumor immune microenvironment and is associated with poor prognosis. BIOCELL. 2023;47:991–1002.
4. Hou B, Zhao L, Zhao T, Yang M, Zhu W, Chen X, Ke X, Ma Z, Gu L, Wang M, Deng M. Chrysophanol inhibits the progression of gastric cancer by activating nod-like receptor protein-3. BIOCELL. 2022;47:175–86.
5. Song J, Xu X, He S, Wang N, Bai Y, Chen Z, Li B, Zhang S. Myristicin suppresses gastric Cancer growth via targeting the EGFR/ ERK signaling pathway. Curr Mol Pharmacol. 2023;16:712–24.
6. Li G, Li F, Wei N, Jia Q. Designing a risk prognosis model based on natural killer cell-linked genes to accurately evaluate the prognosis of gastric cancer. BIOCELL. 2023;47:2081–99.
7. Zhang X, Jin M, Yao X, Liu J, Yang Y, Huang J, Jin G, Liu S, Zhang B. Upregulation of LncRNA WT1-AS inhibits tumor growth and promotes autophagy in gastric Cancer via suppression of PI3K/Akt/mTOR pathway. Curr Mol Pharmacol. 2024;17:10.
8. Fukagawa T, Katai H, Mizusawa J, Nakamura K, Sano T, Terashima M, Ito S, Yoshikawa T, Fukushima N, Kawachi Y, Kinoshita T, Kimura Y, Yabusaki H, Nishida Y, Iwasaki Y, Lee SW, Yasuda T, Sasako M, Stomach Cancer Study Group of the Japan Clinical Oncology Group. A prospective multi-institutional validity study to evaluate the accuracy of clinical diagnosis of pathological stage III gastric cancer (JCOG1302A). Gastric Cancer. 2018;21:68–73.
9. Zhang W, Guang Y, Zhang Y, Wang J, Jin K, Liu Y, Wang F, Yu W, Zhang H, Li G, Yu D, Chen H, Xu Q, Sun B. Effect of lymph nodes count in node-positive gastric cancer. J Cancer. 2019;10(23):5646–53.
10. Amin MB, Greene FL, Edge SB, Compton CC, Gershenwald JE, Brookland RK, Meyer L, Gress DM, Byrd DR, Winchester DP. The eighth edition AJCC Cancer staging manual: continuing to build a Bridge from a population-based to a more personalized approach to cancer staging. CA Cancer J Clin. 2017;67:93–9.
11. Lordick F, Carneiro F, Cascinu S, Fleitas T, Haustermans K, Piessen G, Vogel A, Smyth EC, ESMO Guidelines Committee. Gastric cancer: ESMO clinical practice guideline for diagnosis, treatment and follow-up. Ann Oncol. 2022;33:1005–20.
12. Hwang SW, Lee DH, Lee SH, Park YS, Hwang JH, Kim JW, Jung SH, Kim NY, Kim YH, Lee KH, Kim HH, Park DJ, Lee HS, Jung HC, Song IS. Preoperative staging of gastric cancer by endoscopic ultrasonography and multidetector-row computed tomography. J Gastroenterol Hepatol. 2010;25:512–8.
13. Wang Y, Liu W, Yu Y, Liu JJ, Xue HD, Qi YF, Lei J, Yu JC, Jin ZY. CT radiomics nomogram for the preoperative prediction of lymph node metastasis in gastric cancer. Eur Radiol. 2020;30:976–86.
14. Yang Y, Chen H, Ji M, Wu J, Chen X, Liu F, Rao S. A new radiomics approach combining the tumor and peri-tumor regions to predict lymph node metastasis and prognosis in gastric cancer. Gastroenterol Rep (Oxf). 2023;7:goac080.
15. Xu X, Zheng G, Zhang T, Zhao Y, Zheng Z. Clinical significance of metastasis or micrometastasis to the lymph node along the superior mesenteric vein in gastric carcinoma: A retrospective analysis. Front Oncol. 2021;11:707249.
16. Gao X, Ma T, Cui J, Zhang Y, Wang L, Li H, Ye Z. A radiomics-based model for prediction of lymph node metastasis in gastric cancer. Eur J Radiol. 2020;129:109069.
17. Wang L, Gong J, Huang X, Lin G, Zheng B, Chen J, Xie J, Lin R, Duan Q, Lin W. CT-based radiomics nomogram for preoperative prediction of 10 lymph nodes metastasis in advanced proximal gastric cancer. Eur J Surg Oncol. 2021;47(6):1458–65.
18. Feng QX, Liu C, Qi L, Sun SW, Song Y, Yang G, Zhang YD, Liu XS. An intelligent clinical decision support system for preoperative prediction of lymph node metastasis in gastric Cancer. J Am Coll Radiol. 2019;16:952–60.
19. Dong D, Fang MJ, Tang L, Shan XH, Gao JB, Giganti F, Wang RP, Chen X, Wang XX, Palumbo D, Fu J, Li WC, Li J, Zhong LZ, De Cobelli F, Ji JF, Liu ZY, Tian J. Deep learning radiomic nomogram can predict the number of lymph node metastasis in locally advanced gastric cancer: an international multicenter study. Ann Oncol. 2020;31:912–20.
20. Ye Z, Zeng D, Zhou R, Shi M, Liao W. Tumor microenvironment evaluation for Gastrointestinal Cancer in the era of immunotherapy and machine learning. Front Immunol. 2022;13:819807.
21. Wei R, Zhuang Y, Wang L, Sun X, Dai Z, Ge Y, Wang H, Song B. Histogram-based analysis of diffusion-weighted imaging for predicting aggressiveness in papillary thyroid carcinoma. BMC Med Imaging. 2022;22:188.
22. Tan CH, Vikram R, Boonsirikamchai P, Bhosale P, Marcal L, Faria S, Charnsangavej C. Extramural venous invasion by Gastrointestinal malignancies: CT appearances. Abdom Imaging. 2011;36:491–502.
23. Li J, Xu S, Wang Y, Fang M, Ma F, Xu C, Li H. (2023) Spectral CT-based nomogram for preoperative prediction of perineural invasion in locally advanced gastric cancer: a prospective study. Eur Radiol. 2023;33(7):5172–5183. https://doi.org/10.1007/s00330-023-09464-9. Epub 2023 Feb 24. Erratum in: Eur Radiol 33:5207.
24. Li J, Zhang C, Wei J, Zheng P, Zhang H, Xie Y, Bai J, Zhu Z, Zhou K, Liang X, Xie Y, Qin T. Intratumoral and peritumoral radiomics of Contrast-Enhanced CT for prediction of Disease-Free survival and chemotherapy response in stage II/III gastric Cancer. Front Oncol. 2020;10:552270.
25. Komori M, Asayama Y, Fujita N, Hiraka K, Tsurumaru D, Kakeji Y, Honda H. Extent of arterial tumor enhancement measured with preoperative MDCT gastrography is a prognostic factor in advanced gastric cancer after curative resection. AJR Am J Roentgenol. 2013;201:W253–61.
26. Yang J, Wu Q, Xu L, Wang Z, Su K, Liu R, Yen EA, Liu S, Qin J, Rong Y, Lu Y, Niu T. Integrating tumor and nodal radiomics to predict lymph node metastasis in gastric cancer. Radiother Oncol. 2020;150:89–96.
27. Liu S, Liu S, Ji C, Zheng H, Pan X, Zhang Y, Guan W, Chen L, Guan Y, Li W, He J, Ge Y, Zhou Z. Application of CT texture analysis in predicting histopathological characteristics of gastric cancers. Eur Radiol. 2017;27:4951–9.
28. Guo Q, Sun Q, Bian X, Wang M, Dong H, Yin H, Dai X, Fan G, Chen G. Development and validation of a multiphase CT radiomics nomogram for the preoperative prediction of lymphovascular invasion in patients with gastric cancer. Clin Radiol. 2023;78:e552–9.
29. Jiang Y, Chen C, Xie J, Wang W, Zha X, Lv W, Chen H, Hu Y, Li T, Yu J, Zhou Z, Xu Y, Li G. Radiomics signature of computed tomography imaging for prediction of survival and chemotherapeutic benefits in gastric cancer. EBioMedicine. 2018;36:171–82.
30. Ajani JA, In. In: Sano H, editor. AJCC Cancer staging Manual.8thed. Adv Anat Pathol; 2016.

31. Li J, Xu S, Wang Y, Fang M, Ma F, Xu C, Li H. Spectral CT-based nomogram for preoperative prediction of perineural invasion in locally advanced gastric cancer: a prospective study. Eur Radiol. 2023;33:5172–83.
32. Sandri M, Zuccolotto P. Data analysis, classification and the forward search. Berlin Heidelberg: Springer; 2006.
33. Gao X, Ma T, Cui J, Zhang Y, Wang L, Li H, Ye Z. A CT-based radiomics model for prediction of lymph node metastasis in early stage gastric Cancer. Acad Radiol. 2021;28:e155–64.
34. Jiang Y, Wang H, Wu J, Chen C, Yuan Q, Huang W, Li T, Xi S, Hu Y, Zhou Z, Xu Y, Li G, Li R. Noninvasive imaging evaluation of tumor immune microenvironment to predict outcomes in gastric cancer. Ann Oncol. 2020;31(6):760–8.
35. Sun Z, Zhang TJ, Ahmad MU, Zhou ZX, Qiu L, Zhou KN, Xiong WJ, Xie JJ, Zhang ZC, Chen CL, Yuan QY, Chen Y, Feng WY, Xu YK, Yu LQ, Wang W, Yu J, Li GX, Jiang YM. Comprehensive assessment of immune context and immunotherapy response via noninvasive imaging in gastric cancer. J Clin Investig. 2024;134(6):e175834.
36. van Griethuysen JJM, Fedorov A, Parmar C, Hosny A, Aucoin N, Narayan V, Beets-Tan RGH, Fillion-Robin JC, Pieper S, Aerts HJWL. Computational radiomics system to Decode the radiographic phenotype. Cancer Res. 2017;77:e104–7.
37. Lee CM, Cho JM, Jang YJ, Park SS, Park SH, Kim SJ, Mok YJ, Kim CS, Kim JH. Should lymph node micrometastasis be considered in node staging for gastric cancer? The significance of lymph node micrometastasis in gastric cancer. Ann Surg Oncol. 2015;22:765–71.
38. Sun Z, Jiang Y, Chen C, Zheng H, Huang W, Xu B, Tang W, Yuan Q, Zhou K, Liang X, Chen H, Han Z, Feng H, Yu S, Hu Y, Yu J, Zhou Z, Wang W, Xu Y, Li G. Radiomics signature based on computed tomography images for the preoperative prediction of lymph node metastasis at individual stations in gastric cancer: A multicenter study. Radiother Oncol. 2021;165:179–90.
39. Shin J, Lim JS, Huh YM, Kim JH, Hyung WJ, Chung JJ, Han K, Kim S. A radiomics-based model for predicting prognosis of locally advanced gastric cancer in the preoperative setting. Sci Rep. 2021;11:1879.
40. Zeng Q, Li H, Zhu Y, Feng Z, Shu X, Wu A, Luo L, Cao Y, Tu Y, Xiong J, Zhou F, Li Z. Development and validation of a predictive model combining clinical, radiomics, and deep transfer learning features for lymph node metastasis in early gastric cancer. Front Med (Lausanne). 2022;9:986437.
41. Tsurumaru D, Miyasaka M, Muraki T, Asayama Y, Nishie A, Oki E, Hirahashi M, Hida T, Honda H. Diffuse-type gastric cancer: specific enhancement pattern on multiphasic contrast-enhanced computed tomography. Jpn J Radiol. 2017;35(6):289–95.
42. Gao XJ, Ma T, Cui J, Zhang Y, Wang L, Li H, Ye Z. A radiomics-based model for prediction of lymph node metastasis in gastric cancer. Eur J Radiol. 2020;129:109069.
43. Ji X, Bu ZD, Yan Y, Li ZY, Wu AW, Zhang LH, Zhang J, Wu XJ, Zong XL, Li SX, Shan F, Jia ZY, Ji JF. The 8th edition of the American joint committee on Cancer tumor-node-metastasis staging system for gastric cancer is superior to the 7th edition: results from a Chinese mono-institutional study of 1663 patients. Gastric Cancer. 2018;21:643–52.

Publisher's note